Comparison Study of Rotor Structures of Doubly Excited Brushless Reluctance Machine by Finite Element Analysis

Longya Xu
Member, IEEE

Yifan Tang and Lurong Ye
Student Member, IEEE

The Ohio State University
Department of Electrical Engineering
2015 Neil Avenue
Columbus, Ohio 43210

Abstract: Doubly Excited Brushless Reluctance Machine (DEBRM) has gained much attention recently in the area of variable-speed constant-frequency generating systems and adjustable speed drives. Two types of reluctance rotor structure, axially laminated and simple salient rotors, are suggested in the DEBRM development. Due to the unconventional pole number combination of the stator and rotor, performance evaluation of the DEBRM with different rotor structures is difficult. A comparison study of two rotor structures of the DEBRM is presented in this paper by finite element analysis. It is shown that by calculating self- and mutual-flux linkage of the dual stator windings as the function of rotor positions, performance of the complicated DEBRM can be evaluated conveniently. Various advantages and disadvantages of the DEBRM associated with the two rotor structures are also discussed.

Keywords: induction machine, reluctance machine, doubly excited, self-cascaded, brushless, Hunt machine, axially laminated rotor

Introduction

Doubly Excited Brushless Reluctance Machine (DEBRM) has experienced a long history of development. Starting at the turn of this century, Hunt proposed a doubly fed self-cascaded induction machine to emulate the operational characteristics of a conventional cascaded induction machine[1]. Of his machine, the basic structure featuring dual stator winding of different pole numbers wound in a common stator core with a cage rotor has been proposed. Although the so-called Hunt machine took its very primitive form in the early days, the operational feasibility of the doubly fed machine has been demonstrated. In the 60s and 70s, Broadway gave a more detailed analysis of a similar type machine[2]. More significantly, Broadway analyzed the function of the short-circuit cage rotor and suggested the possibility of using an axially laminated reluctance rotor in place of the short-circuit cage one. In effect, the study of self-cascaded induction machine had given starting to the development of doubly excited reluctance machine. Although the DEBRM gained its own identity since then, which is substantially different from its ancestor–the cascaded induction machine, the theory of such a machine had not progressed. In most cases, derivation of the machine models have been semi-intuitive with modification of the conventional induction and synchronous machine of rotating flux. Results presented, therefore, were very approximated and some were inconsistent. For example, the substantial harmonics of airgap flux space generated by the interaction of stator MMF and rotor with different pole number had never been explained. In addition, the coefficient accounting for the mutual coupling between the two sets of stator winding become negative, a vague and unexplainable result[2].

93 WM 012-5 EC A paper recommended and approved by the IEEE Electric Machinery Committee of the IEEE Power Engineering Society for presentation at the IEEE/PES 1993 Winter Meeting, Columbus, OH, January 31 - February 5, 1993. Manuscript submitted August 28, 1992; made available for printing November 3, 1992.

The lack of proper theory and modeling had retarded further development of the DEBRM for many years until recently. In the past decade, interests in the doubly fed brushless machine with both cage rotor and reluctance rotor have been renewed due to a rapid development in power electronics converter. Coupled with the power electronics converter as the core components, the doubly excited brushless machine appears very attractive for its rugged structure, the good compatibility with power converter, and the flexible operational mode. In constructing a variable speed drive and variable-speed constant-frequency generating system, the doubly excited brushless is potential to achieve high efficiency, low cost, enhanced reliability and flexible control. The synchronous machine version of the Broadway concept was implemented as a high efficiency machine by Heyne and El-antably [4]. Various efforts have also been made to establish a proper dynamic model and explore its design variations [5,6,7,8].

In our previous work we have presented a throughout analysis on the transient behavior of the DEBRM[5]. The analysis started from the physical description of the machine and abandoned completely the ideas of treating the DEBRM as a conventional rotating flux machine, accounting for only the fundamental flux component [2]. Instead, by treating the DEBRM on its own right, the mutual coupling between the two stator windings, and the interaction between the stator MMFs and the rotor saliency have been fully described. The pulsating flux of the DEBRM has been taken into consideration. As the results of the analysis, the underlying mechanism that the DEBRM could resemble a synchronous or induction machine emerged. The work has also pointed out that any electric machine with similar features would equally result in electromechanical conversion. The operational constraints regarding the DEBRM and the alike were discussed in [6]. The DEBRM has been further studied by finite element method to include nonlinearity and to explore the alternative pole number combination of the stator and rotor[9]. Application and field orientation control of the DEBRM in variable-speed constant-frequency generating system are presented in [10].

Parallel to the analysis of the DEBRM, the doubly excited brushless machine with cage rotor has been investigated by A. Wallace and his associates [7,8]. In their work, a similar approach of [5] is applied and various winding arrangements are studied. The dynamic model of cage-rotor Doubly Excited Brushless Machine is established and the possibility of operating the machine in variable speed drives is investigated. Their work also indicated that the Doubly Excited Brushless Machine is such a machine that analysis by the conventional rotating flux theory is irrelevant.

Recognizing the fact that in DEBRM the MMFs established by the stator windings are constantly modulated by the rotor permeance of different pole number, we believe that similar interactions between the stator MMFs and any other type reluctance rotor could also result in electromechanical energy conversion. In such a case, the conventional salient pole rotor appears particularly attractive for its very simple structure and the inherent immunity to the iron losses. However, for an optimal design of a DEBRM with salient pole rotor, critical questions have to be answered regarding the machine torque capability, power density and torque ripple.

In this paper, a finite element analysis is presented to

investigate the DEBRM with two different rotor structures. The main purposes of using finite element method is to overcome the difficulties in dealing with the unconventional geometry and winding connection, to consider magnetic nonlinearity, and to verify the postulations from the simplified linear analysis. First, the geometry of the DEBRM is directly described by a discretized nonlinear model in terms of field vector potential. Secondly, the terminal characteristics, the winding flux linkages, are calculated from the field solutions as a function of the rotor positions. Thirdly, the loaded conditions are simulated, and the torque capability and torque ripples are evaluated. Finally, the discussion regarding the advantage and disadvantages of the DEBRM with each type of rotor structure are presented.

Geometry of Rotor Structures

The DEBRM assembly with an axially laminated rotor is shown in Figure 1(a) and another two salient pole rotors for comparison are shown in Figure 1(b) (in later comparison, the three rotors will be refereed to as rotor A, rotor B and rotor C respectively). The major dimensions and the detailed specifications of the DEBRM are given in Table 1. The stator has two sets of three-phase sinusoidally distributed windings. The pole number of one stator winding is p =2 and another q = 4 (referred as 2-pole and 4-pole windings later on). The spatial distribution of the dual windings is described in Figure 2. When the 2-pole and 4-pole windings are doubly excited by two sinusoidal currents at frequencies of ω_1 and ω_2, two rotating MMFs *(not flux)* along the airgap at speed of ω_{1m} and ω_{2m} are generated, where

$$\omega_{1m} = \frac{2\omega_1}{p} \tag{1}$$

and

$$\omega_{2m} = \frac{2\omega_2}{q} \tag{2}$$

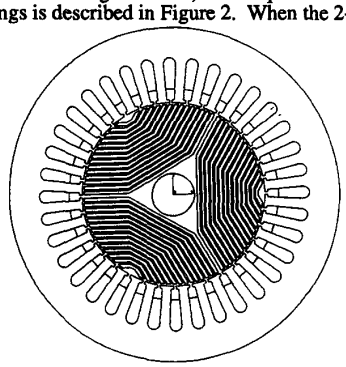

(a) Stator and Axially Laminated Rotor Assembly

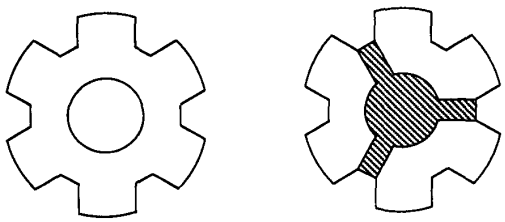

(b) Salient Pole Rotors with and without Flux Barriers

Figure 1 DEBRM Stator and Rotor

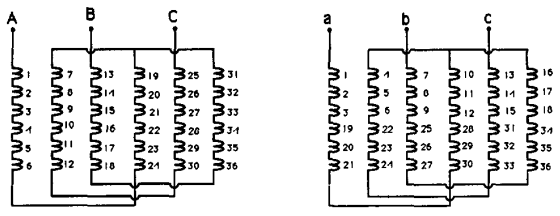

2-pole Winding Distribution 4-pole Winding Distribution

Figure 2 Dual Stator Windings of the DEBRM

The axially laminated rotor (rotor A) consists of 3 pieces of axially laminated segments and the laminations in each segment are interleaved with non-magnetic material as indicated in the figure. Whenever the magnetic flux lines are forced to travel in a path normal to the lamination plane, the flux lines encounter the maximum reluctance. Yet, whenever the flux lines are driven to travel along the lamination plane, the reluctance is minimum.

The first salient pole rotor (rotor B) is a simple laminated style of a conventional synchronous or switched reluctance machine. For the sake of comparison the pole number of the simple salient rotor is chosen to be 6, most analogous to its axially laminated counterpart. The reluctance of the rotor is created by notching the iron material along the q-axis. It is evident that the laminated salient pole rotor has a rugged structure and inherent immunity to the eddy current losses.

The second salient pole rotor (rotor C) has almost the same structure of rotor B except that the laminations are partitioned into three magnetically isolated segments by addition of three flux barriers. The function of the flux barriers will be discussed in the later sections.

As discussed in [4,5], the DEBRM must follow the frequency constraint to produce useful average torque. Assuming that the frequencies of the voltages supplied to 2-pole and 4-pole windings are ω_1 and ω_2 respectively, the rotor speed is governed by the equation:

$$\omega_{mr} = \frac{\omega_1 \pm \omega_2}{(p+q)/2} \tag{3}$$

where ω_{mr} is the mechanical speed of the rotor. In this paper, Eq. (3) will be used as a guideline to choose the frequency of excitation current and the rotor speed.

Field Analysis by the Finite Element Method

In order to analyze the magnetic field of the DEBRM and to relate the terminal characteristics to the complicated airgap flux pattern, the finite element method is chosen to solve for the magnetic field [6]. Assuming a magnetic vector potential, A_z, in the z-direction, the magnetic field of the DEBRM is described by the Poisson Equation:

$$\frac{\partial}{\partial x}\left(\gamma \frac{\partial A_z}{\partial x}\right) + \frac{\partial}{\partial y}\left(\gamma \frac{\partial A_z}{\partial y}\right) = -J_0 \tag{4}$$

where γ is the magnetic reluctivity and J_0 is the excitation current density. In the field analysis, γ is determined by the nonlinear B-H curve and J_0 is determined from the excitation current. Additional assumptions are made: i) the machine is relatively long and the field quantities are invariant in the z-direction; ii) the iron material is not grain-oriented and the B-H curve is single-valued; and iii) the flux lines are confined within the stator core.

As an example, Figure 3 shows the discretized model of the DEBRM with rotor A. To guarantee computation accuracy, more than 4000 elements are contained and in the neighborhood of the airgap elements are dense. An enlargement of the discretized airgap is shown in the same figure. The discretized DEBRM models with rotors B and C are also established with the same assumptions as stated above.

No-Load Operation

It was made clear in [9] that for the DEBRM the no-load condition means *no electromechanical energy conversion when the rotor rotating*, which corresponds to the case of exciting only one

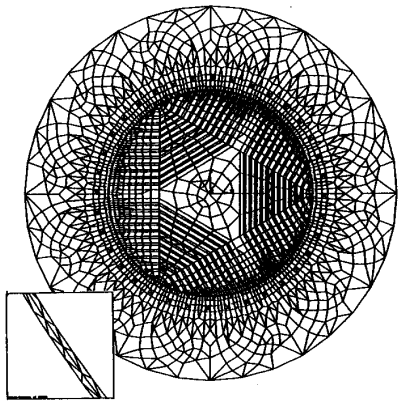

Figure 3 Discretized Field Model of the DEBRM

of the two sets of stator winding. A constant rotor speed is assumed to simulate the mechanical movement of the rotor. The incremental angle of rotor rotation is chosen to be a slot pitch, 10 degrees mechanical.

1) Airgap Flux Distribution

The airgap flux distribution of the DEBRM at no-load can be investigated when the 2-pole or 4-pole winding is excited with a three-phase current at any frequency [9]. However, current at zero frequency (DC) applied to 2-pole winding, the most convenient excitation, is used for simplicity. In this way, a stationary, sinusoidally distributed MMF is created. With the rotor of different pole number, a non-sinusoidal airgap flux is produced. The flux distribution over the cross-section of the DEBRM is shown in Figures 4(a), (b) and(c) corresponding to rotors A, B and C at their initial positions. It is very interesting to note that when rotors A and C are used, the flux lines produced by the stator MMF and the rotor permeance form *three* curls and each of the curls is almost symmetric about its axis. Because each curl occupies 120° span over the cross-section, we may call the flux patterns of rotors A and C 120° symmetric. By contrast, the flux lines with rotor B form only two curls and are 180° symmetric. The difference of the flux patterns created by the rotors stems from their different magnetic structures. Note that for rotor A and C, the flux follows the path provided by the *magnetically isolated laminations with 120° symmetry*. However, for rotor B, all of the six rotor poles are essentially *magnetically short-circuit by a single piece of iron with 180° symmetry*. Therefore, it is not surprising that the flux generated is in 180° symmetry. As it will be made clear later, the fundamental difference of the flux pattern impacts the performance of the DEBRM significantly .

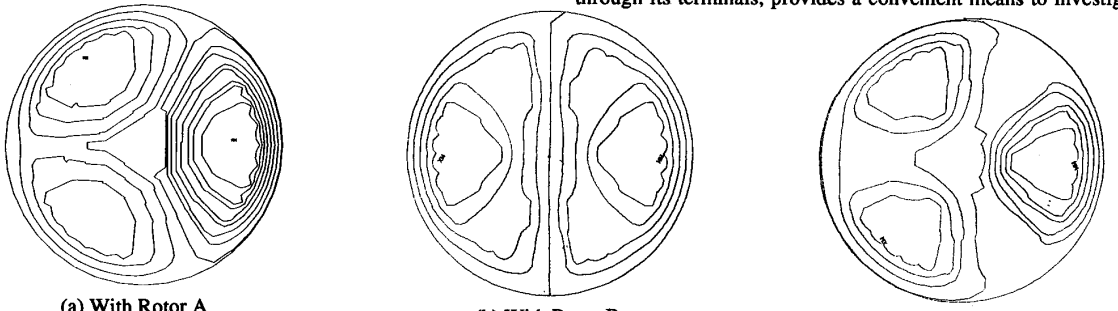

(a) With Rotor A (b) With Rotor B (c) With Rotor C

Figure 4 Flux Distribution over the Cross-Section of DEBRM

As soon as the rotor starts rotating, the rotor permeance will modulate the stator MMF and the flux distribution of the DEBRM will change from that at initial rotor position. Figures 5(a) and (b) shows the airgap flux at 6 different rotor positions spanning 120 degree rotation for rotors A and C. It is interesting to observe that no explicit number of poles or traveling flux wave can be identified from all of the plots. Instead, the airgap flux is featured by the non-sinusoidal, pulsating pattern.

Since both rotors A and C repeat their structures for every 120° in space, the airgap flux repeats the distribution pattern for every 120° rotor rotation as well. This 120° repetition cycle can be identified from the figures. For a non-zero frequency excitation current, or equivalently, for a rotating MMF wave, the flux pattern repetition becomes either less or more frequently than that of the zero frequency excitation, depending on the relative rotating direction and speed of the MMF to that of the rotor. However, the flux patterns shown in the figures will periodically occur. For example, the flux distribution will repeat its pattern for every 120° incremental of the relative displacement between the rotor and the stator MMF. Under such circumstances, it is not essential to emphasize whether the relative displacement is created by the rotor movement, the stator MMF wave movement, or both. It is seen that the airgap flux distribution shown in Figure 5 is still representative for excitation of any frequency at any rotor speed.

By the same method, we have also investigated flux pattern when the 4-pole winding is excited. While the airgap flux pattern is different from that of the 2-pole winding excitation, the features of the nonsinusoidal, pulsating flux distribution remain. Plausibly, one might resort to the harmonic decomposition method that takes the fundamental flux component into account while neglecting the nonessential harmonics. However, the complicity exists even in determining what is the "fundamental component" and what are those "negligible harmonics" for the flux distribution shown in the figures. In effect, it will be made clear in this paper that harmonic decomposition is not a relevant approach for the DEBRM analysis.

2) Winding Flux Linkage

Winding flux linkage, obtained by looking into the winding through its terminals, provides a convenient means to investigate the electromechanical energy conversion of an electric machine. In particular, if the flux linkage of a stator winding varies as the function of the rotor movement, a speed voltage will be induced and electromechanical energy conversion becomes realizable. The flux linkages of the stator winding have been calculated through finite element analysis for the three rotor structures. The method of calculating winding flux linkage from the solution of the vector potential is summarized in Appendix A.

a). Self Flux Linkage

In order to relate the magnetic field analysis to the terminal characteristics, two types of winding flux linkages of the DEBRM are particularly concerned, i.e. the self- and the mutual-flux linkages. For the convenience of analysis, we have the definition of the self- and mutual-flux linkages of the DEBRM slightly different. The *self flux linkage* is defined as: the flux linked by one phase winding when the three-phase winding of the same pole number is excited by a three-phase symmetric current. This so-defined self flux linkage can be visualized as: if an airgap flux is generated by a three-phase winding of common pole number, the

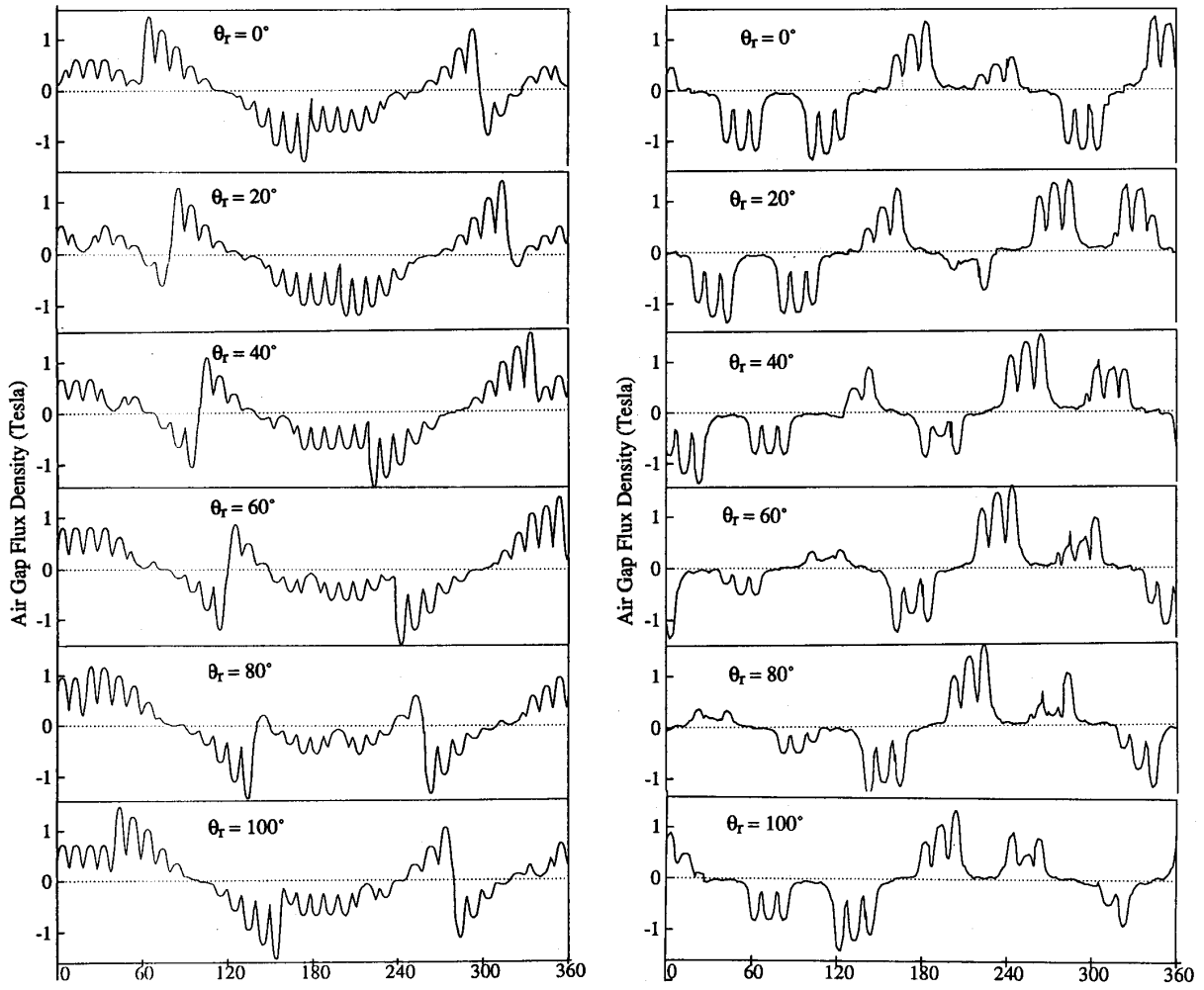

(a) Airgap Flux Distribution with Rotor A

(b) Airgap Flux Distribution with Rotor C

Figure 5 No-Load Airgap Flux Distribution at 6 Rotor Positions

self flux linkage is the flux weighted by a single phase winding in the set. Since the winding flux linkage is a terminal quantity, it is also considered an lumped description of the magnetic flux from the an individual winding point of view.

In Figures 6(a), (b) and (c), the self flux linkages of the 2-pole winding are plotted versus the rotor positions for three different rotors. The self flux linkages of rotors A and C are similar. That is, when the excitation current is DC, the flux linkage of the winding is also DC, independent of the rotor speed and positions. The self flux linkage using rotor B, however, is slightly different and depends on the rotor positions, pulsating six times per rotor revolution.

From the self flux linkage plot , we can derive that if the DEBRM with rotor A or C is singly excited, no flux linkage variation will be experienced by the excited winding as the function of rotor speed. Thus, no induced speed voltage and no electromechanical energy conversion will be possible. If rotor B is used in the DEBRM, the self flux linkage varies six time per rotor revolution and a small AC speed voltage will be induced. However, the DC current and AC speed voltage constitute no average electromagnetic power and torque except energy oscillation. Therefore, from both cases we can conclude that the singly excited DEBRM is, indeed, in no-load condition. Although this conclusions is from the computation of self flux linkage by exciting 2-pole winding only, the same conclusion can be reached by exciting the 4-pole winding only. In addition, AC excitation on either 2-pole or 4-pole winding also gives the same conclusion[9].

b). Mutual Flux Linkage

The *mutual flux linkage* is defined as: the flux linked by one phase winding while the other three-phase winding of different pole number is excited by a three-phase symmetric current. Similarly, the mutual flux linkage can be interpreted as one three-phase winding generated flux weighted by another phase winding of different pole number. It can be predicted that since the pole numbers, or pole pitches of the two sets of winding are different, the self and mutual flux linkages based on the same flux distribution will be substantially different.

In Figures 7(a), the mutual flux linkage of the 4-pole winding is plotted for rotor A with the 2-pole winding being excited by a three-phase current at zero frequency. It very important to note that the mutual flux linkage is closely related to the rotor positions. In effect, Equation (3) relating the frequencies ω_1, ω_2 and ω_{rm} is verifiable by the figure. Under such circumstances a speed voltage will be induced in the 4-pole winding while the rotor is moving. Further, the profile of the mutual flux linkage indicates that the induced speed voltage will be sinusoidal.

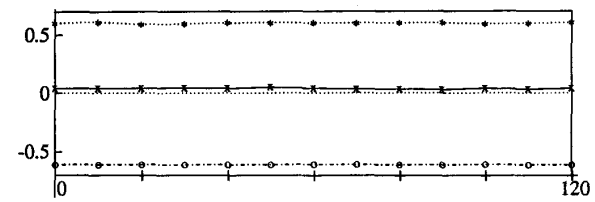

(a) Self Flux Linkage with Rotor A

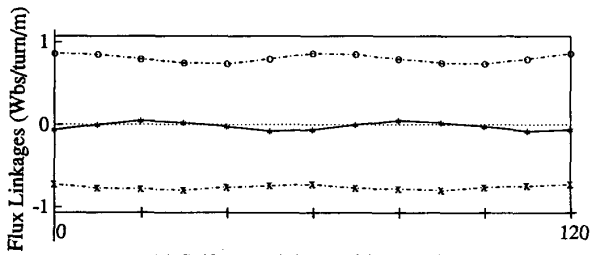

(b) Self Flux Linkage with Rotor B

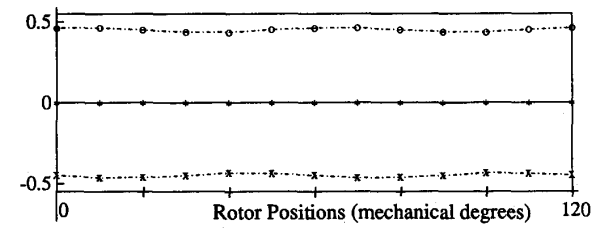

(c) Self Flux Linkage with Rotor C

Figure. 6 Winding Self Flux Linkages versus Rotor Positions

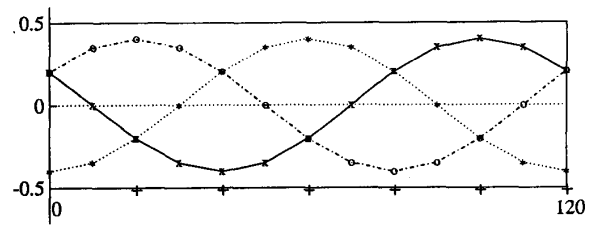

(a) MutualFlux Linkage with Rotor A

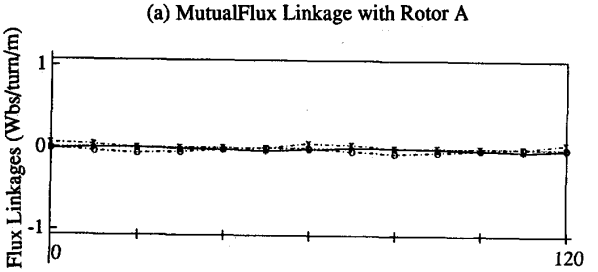

(b) MutualFlux Linkage with Rotor B

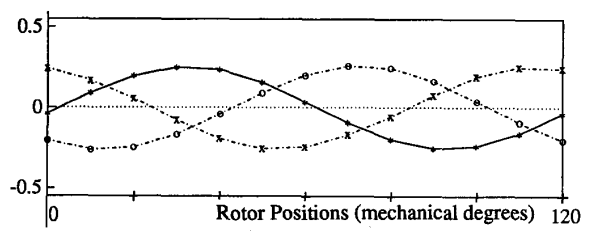

(c) MutualFlux Linkage with Rotor C

Figure. 7 Winding Mutual Flux Linkages versus Rotor Positions

In Figure 7(b), the mutual flux linkage of the 4-pole winding is plotted for rotor B, being identically zero. The result indicates that if a simple salient rotor as rotor B is applied in the DEBRM, no mutual coupling between the 2-pole and 4-pole winding is created and, thus, no induced speed voltage and electromechanical energy conversion can accomplished.

Figure 7(c) shows the mutual flux linkages with rotor C. It is interesting to note that with a much simpler structure than that of rotor A, the mutual flux linkages varies similarly as rotor A is applied. The major difference is that the mutual coupling created by rotor C is substantially lower than that created by rotor A. The low mutual coupling with rotor C can be verified by observing the magnitude of the mutual flux linkage variation for the two rotor cases.

Summarizing the flux linkage calculation, we have qualitatively verified several important conclusions regarding the DEBRM and the magnetic characteristic of the three different rotors:

(1) If it is singly excited the DEBRM will be in no-load condition, no matter what rotor is used;
(2) Simple salient pole rotor (rotor B) is in 180° symmetry and can not create mutual coupling between 2-pole and 4-pole winding;
(3) In order to achieve induced speed voltage, modification of rotor B to rotor C is necessary so that magnetic isolation and 120° symmetry as that of rotor A are created. In this case, mutual coupling is created between the windings of different pole number.
(4) The variation of the mutual flux linkages created by the rotation of rotor A and C is in sinusoidal profile and at the frequency constrained by Equation (3).

Note that in the flux linkage computation we have used the complete solution of the field analysis and exact winding connection. Equivalently, the magnetic non-linearity and all of the space harmonics of the flux are automatically included. If we would have neglected flux harmonics, the results of the flux linkage calculation would be very different. For the convenience of analysis, we have only applied DC to the 2-pole winding to shown the results. It can be shown that excitation at any other frequency applied to either 2-pole or 4-pole winding will obtain the same results.

Comparison of Torque Capability

Up to this point, it is clear that if only one set winding is excited, it is impossible to induce speed voltage in the excited winding so as to realize electromechanical energy conversion. Nevertheless, with rotor A or C, the rotor-position-dependent mutual coupling can be created between the 2-pole and 4-pole windings. As the result of the mutual flux linkage variation, the induced speed voltage is sinusoidal. With rotor B, no mutual coupling between the two stator windings is introduced. In this section, the torque capability are quantitatively investigated for the DEBRM with rotors A and C. Since rotor B can not achieve mutual coupling between the 2-pole and 4-pole windings, it will not be discussed in this section.

1) Principle of Torque Production

If a current of the same frequency as that of the mutual flux linkage variation is injected into the winding, an electromagnetic torque will be produced. The general form of the torque is:

$$T_e = \frac{3 E_p I_p \cos\phi + 3 E_q I_q \cos\phi}{\omega_{rm}}$$

$$= \frac{3\omega_1 \lambda_{mq} I_p \sin\phi + 3\omega_2 \lambda_{mp} I_q \sin\phi}{\omega_{rm}}$$

$$= \frac{3}{2}(p+q)\,\lambda_{mq} I_p \sin\phi \qquad (5)$$

where the E_p and E_q are the induced speed voltages associated with the variations of the mutual flux linkages; I_p and I_q are the phase currents; ϕ is the angle between the induced speed voltage and the current; λ_{mp} and λ_{mq} are the mutual flux linkages under the given currents. Note that in the torque derivation, the relation $\lambda_{mp}/\lambda_{mq} = I_p/I_q$ is used and the frequency constraint given in Equation (3) is observed.

Note that if the phase current I_p is injected in phase with respect to the induced speed voltage E_p, or equivalently, orthogonal to the variation of the mutual flux linkage λ_{mq}. A maximum torque production for the given currents is expected. The orthogonal current injection with respect to the mutual flux linkage is actually the field orientation concept similar to that in a synchronous machine operation. Further, the current injection is oriented to the mutual flux linkage variation which, in turn, varies as a function of the rotor positions. Therefore, the orthogonal current injection can be actually implemented by using the rotor positions as reference signal.

2) Evaluation of Torque Capability

With both 2-pole and 4-pole windings doubly excited, and the current through the 4-pole winding orthogonal to its mutual flux linkage, the vector potential and the total flux linkage of the winding are re-calculated. As indicated in Table 1, the main dimensions of the DEBRM are chosen to be those of an induction machine rated at 7.5 hp with the synchronous speed of 1800 rpm.

Using the rated current of the induction machine as the base current, torque production of the DEBRM is evaluated at three current levels for rotors A and C. The resultant phase flux linkage variation and the current of the 4-pole winding are plotted versus the rotor positions in Figures 8(a) and (b). It can be seen that the flux linkage of the winding is no longer orthogonal to the current. Realize that when the DEBRM is doubly excited, the magnetic vector potentials are determined by the currents through both the 2-pole and 4-pole winding and so is the flux linkage. Therefore, the flux linkage of the winding at load contains not only the mutual flux component but also the self flux component resulting in the phase angle shifting and magnitude variation as shown in the figures.

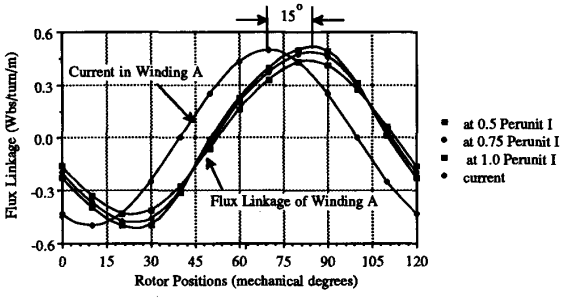

(a) Flux Linkage and Current of Phase A with Rotor A

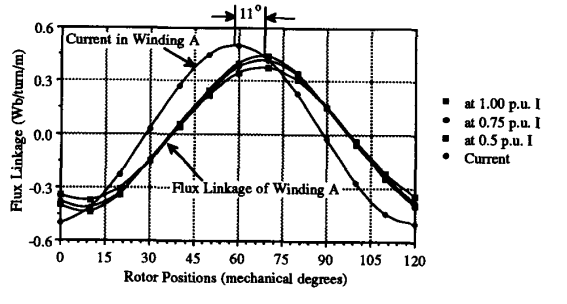

(b) Flux Linkage and Current of Phase A with Rotor C

Figure 8 Phase Angle Between Current and Flux at Load

Based on the calculated flux linkage of the winding shown in Figure 8 the torque production of the DEBRM can be evaluated directly by the electrical and mechanical power balance:

$$T_e = \frac{3\,V_p\,I_p \cos\theta}{\omega_{rm}}$$

$$= \frac{3}{2}(p+q)\,\lambda_p\,I_p \sin\theta \qquad (6)$$

where the V_p and I_p are the phase voltage and current; θ is the angle between the phase voltage and the current; λ_p is the total flux linkage including the mutual and self flux linkage components. It can be shown that if saturation is not considered, Eqs. (5) and (6) are equivalent.[9]

The torque capability of the DEBRM is shown in Figure 9.

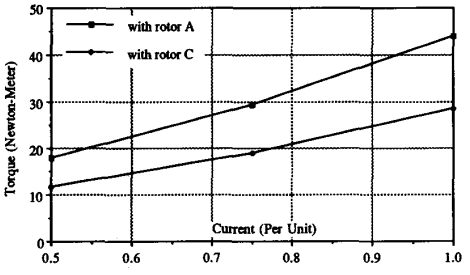

Figure 9 Comparison of the Torque Capability

It is seen that at the same current level, or at the same level of conduction losses, the torque production of the DEBRM with rotor C is about 65% of that with rotor A. From the comparison, it is clear that the torque capability of the DEBRM with rotor A is substantially higher than that of the DEBRM with rotor C. By inspecting the flux linkage profile with rotors A and C at no-load (Figure 6) and loaded (Figure 8) conditions, we can attribute the reduced torque capability of the DEBRM with rotor C to two major reasons: 1). With rotor C, the magnetic structure of the DERBM is less effective to produce winding flux linkages. This is made apparent by the flux linkage magnitude for the two rotor cases at no load condition. 2) With rotor C, the mutual coupling is weaker than the case with rotor A. This is made apparent by the ratio of the self to the mutual flux linkages. Also, the larger angle shifting (58°) of the winding flux linkage from no-load to loaded condition with rotor C than that (45°) with rotor A indicates the dominance of the self flux over the mutual flux component.

Conclusions

The complicated flux distribution inside the DEBRM, coupled with the magnetic nonlinearity, and the less straight forward terminal characteristics of the DEBRM have been investigated in detail by the finite element method for different rotor structures. The following conclusions have been reached by the analysis:

1) Among the three rotors, the axially laminated rotor provide highest mutual coupling between the stator windings of different pole number, and thus, achieve high a torque capability.

2) Simple salient pole rotor can not introduce rotor-position-dependent mutual coupling to the stator windings of different pole number.

3) Modified salient pole rotor with magnetic barriers has almost the same magnetic characteristics as that of the axially laminated rotor except the lower production of flux and mutual coupling.

In spite of the fact that rotor A outperformed rotor C for torque production, rotor C does have several advantages over rotor A: i) the structure is very simple and rugged. The advantage is very attractive because it makes rotor C very cost effective and reliable. ii) since rotor C is made of conventional laminations, low iron losses are guaranteed. Further optimization of rotor C by finite element analysis and research of control strategy are currently in progress and the results will be presented in a future paper.

Acknowledgment

The work presented in this paper is supported by a Research Initiation Grant ESC-9111256 from National Science Foundation.

References

[1] L.J. Hunt, "The Cascade Induction Motor," J. IEE Vol. 52, pp. 406-426, 1914.

[2] A.R.W. Broadway, "Cageless Induction Motor", Proc. IEE, vol. 118, pp. 1593-1600, 1971.

[3] A.R.W. Broadway and G. Thomas, "Brushless Cascade Alternator", Proc. IEE, vol 121, pp. 1529-1535, 1974.

[4] C.J. Heyne and A.M. El-Antably, "Reluctance and Doubly-Excited Reluctance Motors", Final Report, Oak Ridge National Laboratories, Report ORNL/SUB/81-95013/1, 123 pp.

[5] L. Xu, F. Liang, and T. A. Lipo, "Transient Model of the Doubly Fed Reluctance Motor", IEEE Power Engineering Society Summer Meeting, Minneapolis, June, 1990.

[6] L. Xu, F. Liang and T. A. Lipo, "Analysis of a New Variable Speed Doubly Excited Reluctance Motor", Proceedings of International Conference on Electric Machines, presented at MIT Boston, July, 1990.

[7] R. Li, A. Wallace, and Rene Spee, "Dynamic Simulation of Brushless Doubly-Fed Machines", IEEE Transaction on Energy Conversion, Vol. 6, No. 3 September, 1991, pp. 445-451

[8] R. Li, A. Wallace, Rene Spee and Y. Wang, "Two-Axis Model Development of Cage-Rotor Brushless Doubly-Fed Machines", IEEE Transaction on Energy Conversion, Vol. 6, No. 3 September, 1991, pp. 453-460

[9] L. Xu, "Analysis of a Doubly-Excited Brushless Reluctance Machine by Finite Element Method", IEEE Industry Application Society Annual Meeting, 1992, Houston

[10] L. Xu, Y. Tang "A Novel Wind-Power Generating System Using Field Orientation Controlled Doubly-Excited Brushless Reluctance Machine", IEEE Industry Application Society Annual Meeting, 1992, Houston

Table 1

Specifications of the DEBRM

Ratings
Power rating: 5.0 hp
Synchronous Speed: 1200 rpm
Rated Voltage: 160 volts
Rated Current in Primary: 10 amps
Rated Current in Secondary: 10 amps

The main dimensions of the DEBRM are chosen to be the same as those of an induction machine as listed in the following:

Ratings
Power rating: 7.5 hp
Rated Speed: 1750 rpm
Rated Voltage: 230 volts
Rated Current: 10 amps
Power Factor at Rated Load: 0.8

Main Dimensions
Stator Lamination OD: 9.001 in
Stator Lamination ID: 4.954 in
Effective Length of Stator Stack: 4.00 in

APPENDIX A

Consider a single turn coil in a 2-D magnetic field described by the vector potential, A_z, as shown in Figure A-1. The flux linkage of the single-turn coil may be evaluated from the magnetic vector potential A_z as:

$$\lambda_{coil} = L \int_{a_1}^{a_2} B \, d\ell$$

$$= L \int_{a_1}^{a_2} \frac{\partial A}{\partial \ell} d\ell = A_z(a_1) - A_z(a_2) \qquad (5)$$

where $A_z(a_1)$ and $A_z(a_2)$ are the vector potentials at the locations of the coil two sides, a_1 and a_2. L is the effective length of the coil experiencing the flux variation. If the coil has N turns at the same location, the flux linkage will be N times as large. Further, if a winding is formed by several coils connected in series at different locations, the total flux linkage of this winding will be the sum of the flux linkage associated with each individual coil.

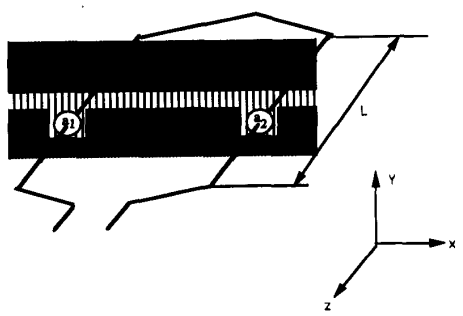

Figure A-1 Coil Flux Linkage Evaluation from Vector Potential

Longya Xu was born in Hunan, China. He graduated from Shangtan Institute of Electrical Engineering in 1970. He received the B.E.E. from Hunan University, China, in 1982, and M.S. and Ph. D. from the University of Wisconsin, Madison, in 1986 and 1990.

From 1971-1978 he participated in 150 kvA synchronous machine design, manufacturing and testing in China. From 1982-1984, he worked as a researcher for linear electric machines in the Institute of Electrical Engineering, Sinica Academia of China. Since he came to the U.S., he has served as a consultant to several industry companies including Raytheon Co., US Wind Power Co., Pacific Scientific Co., and Unique Mobility Inc. for various industrial concerns. He joined the Department of Electrical Engineering at the Ohio State University in 1990, where he is presently an Assistant Professor. Dr. Xu received the 1990 First Prize Paper Award in the Industry Drive Committee, IEEE/IAS. His research and teaching interests include dynamic modeling and converter optimized design of electrical machines and drive systems. He is a member of Electrical Machinery Committee of IEEE/PES, and a member of Industry Drive and Electric Machine Committees of IEEE/IAS.

Lurong Ye received the B.E. and M.S. degrees in Electrical Engineering from Shanghai Jiao Tong University, Shanghai, China, in 1982 and 1987 respectively. From 1982 to 1984, he worked as an electrical engineer in Zai-Bai power plant in Shanghai. After his graduation, he joined this university as a lecturer from 1987 to 1991. In 1988-1989, he was a senior electrical engineer in Sino-Hongkong De-Yi Electrical Company, and a senior electrical engineer in Sino-Hongkong Wei-Da Medical Instrument Co. in 1989-1991. Currently, he is studying in the Department of Electrical Engineering at Ohio State University as an graduate student. His research interests include power electronics, electrical drives and electric machine design.